MILITARY TECHNICAL COLLEGE
CAIRO - EGYPT

7th INTERNATIONAL CONF. ON
AEROSPACE SCIENCES &
AVIATION TECHNOLOGY

ANALYSIS OF THE MECHANICS OF NORMAL PERFORATION OF METALLIC PLATES BY HIGH-SPEED PROJECTILES

by

A. M. Riad *

ABSTRACT

An analytical model that considers the projectile deformation has been developed to describe the plugging process due to the impact of high speed projectiles into metallic plates of finite thicknesses. Both projectile and target materials are considered as strain rate independent and are rigid/plastic linear work hardening with respect to nominal stress-engineering strain relationships. The model identifies two projectile modes: heading and rigid. For each projectile mode, the target perforation process is described consisting of the following stages: (i) erosion, (ii) indentation, (iii) plug formation, and (iv) plug ejection. The plastic wave theory is used with the equations of motion to predict the sequence of the perforation stages of the different projectile modes that represent the complete perforation process of metallic plates.

The model is capable of predicting the time histories of target resisting force, velocity of different moving masses, and projectile penetration depth through the target. It can also estimate the projectile residual velocity, the plug thickness and the final length of projectile after perforation. For each impact velocity, the initial interface area of the projectile front is the only empirical factor in the analysis which is needed to run the model. The model predictions are compared with the experimental results of other investigators; good agreement is obtained. In addition, two thicknesses of LY12-CZ aluminium alloy plates are used as targets to specify the perforation process due to their impact by steel projectiles with velocity range up to 650 m/s. Predicted samples of the model results are presented. The model is also used to discuss the influence of projectile deformation on the different predicted time histories and post perforation results.

KEY WORDS

- Dynamics
- Solid Mechanics
- Impact Dynamics
- Penetration Mechanics
- Impact of Solids

* Dept. Mech. Engng., M. T. C., Cairo, Egypt.

INTRODUCTION

Various analytical models were developed to analyze the perforation process of metallic plates by projectiles. Early models of plate plugging assumed that the projectile and plug were not deformed and moved with the same velocity during perforation; these models described the perforation process in a single stage (e.g. Recht and Ipson [1]). Another class of models which considered the projectile deformation were developed. For instance, Recht [2] considered the projectile deformation within the plug penetration model. He utilized Taylor's concept [3] to model projectile deformation, projectile mass loss and plate deformation.

In the last three decades, multistage perforation models have been developed. A simple two-stage model was presented by Awerbuch [4]; this was modified by Awerbuch and Bodner [5]. The penetration theory of Awerbuch and Bodner consists of three interconnected stages. Various parameters in both models must be determined experimentally. Another two models which describe phenomenologically the plugging process in thin and intermediate thick metallic plates were developed by Liss et al. [6] and Ravid and Bodner [7]. The first model uses for the target material a strain rate independent constitutive relation; whereas the second uses one that is strain rate sensitive. Both models divide the penetration process into five interconnected stages.

Yuan et al. [8] developed a one-dimensional wave propagation model of the plate perforation by cylindrical projectiles. Their theory identified three projectile modes: erosion, flattening and rigid. It also defined two stages with respect to plug motion: (a) formation, and (b) ejection. Plastic deformation at the impact end of the projectile produces a mushroom head that increases the diameter of the plug punched from the plate. Yuan et al. [8] assumed that: (i) the target material is rigid-perfectly plastic, and (ii) the shear stress acts over the surface of the plug deformed section.

The present investigation is an analysis of the perforation process including projectile deformation. The model identifies two projectile modes: heading and rigid. For each projectile mode, the target perforation stages are: (i) erosion, (ii) indentation, (iii) plug formation, and (iv) plug ejection. The projectile and target materials are assumed to be rigid/plastic linear work hardening and the ultimate shear stress is assumed to act on the whole surface of the formed plug.

In the following analysis, the plastic wave theory specified by Lee and Wolf [9] is used to divide the plug material ahead of projectile as well as the projectile material itself into deformed and non-deformed masses. The main equations describing each perforation stage are derived. These equations are compiled into a computer program. The input data consist of projectile diameter, length, density, Brinell hardness number and impact velocity as well as target thickness, density, Brinell hardness number and the constrained factor that includes the effect of the surrounding target material. For each plate thickness, an empirical equation representing the change of initial interface area of the projectile front with impact velocity is fed into the program.

The present model is capable of predicting the time histories of projectile penetration depth through the target, velocity of the moving masses, and target resisting force; it can also estimate the projectile residual velocity, plug thickness, and the final length of projectile after perforation. Moreover, a comparison between the different time histories and post-perforation results when the projectile deformation is considered and when the projectile is assumed to be rigid during target penetration is presented and discussed.

MAIN ASSUMPTIONS

To simplify the perforation process, several assumptions have been used in the present model. The main assumptions are introduced; the rest are elaborated during the model formulation. The main assumptions are:

(i) Deformations of the projectile front and target material ahead of projectile are associated with the propagation of the plastic waves from the interface through their materials, respectively. Erosion accompanies the target surface when the penetration velocity is greater than the plastic wave velocity through the target material.

(ii) The target is infinitely wide to eliminate any influence of boundary conditions on perforation.

(iii) No thermal effect is considered; the model neglects the heat energy loss and the effect of temperature on material properties.

(iv) The projectile front during the heading mode is completely in-contact with the target. The projectile contact area is assumed to be constant during the perforation process.

(v) The friction due to contact between the projectile and hole vacated by the plug is neglected.

(vi) The shear stress acts over the surface of the ejected plug that is in contact with the surrounding target material. The ejected plug has a cross-sectional area equal to the cross-sectional area of the projectile front.

PROJECTILE AND TARGET MATERIALS

Projectile and target materials are assumed to be compressible and to have rigid/plastic linear work hardening constitutive equations. It has been suggested by Recht [2] that the dynamic compressive nominal stress-engineering strain relationship for common metal alloys can be represented in the region of plastic deformation by:

$$\sigma = \sigma_i + B_i \epsilon, \quad i = P, t \tag{1}$$

where

$$\sigma_i \ [MPa] = 3.92 \ x \ (HB)_i, \tag{1a}$$

and

$$B_i \ / \ \sigma_i = 2.6 \ . \tag{1b}$$

σ_i is the dynamic yield stress, B_i is the dynamic work hardening coefficient, $(HB)_i$ is the Brinell hardness number, and subscripts P and t denote the projectile and target, respectively. σ and ϵ are the nominal stress and the plastic strain, respectively.

The generation of normal strain in the target material requires more stress under the constrained uniaxial conditions. The required stress has been determined by many investigators [8, 10, 11]. In the present model, the uniaxial constrained dynamic yield stress of the target σ_c is taken to be equal to 2.7 σ_t [10]. Then the constitutive equation that represents the target material is rewritten as:

$$\sigma = \sigma_c + B_t \epsilon \ , \tag{2}$$

where σ is the constrained dynamic stress, and σ_C is the constrained dynamic yield stress. The plastic wave velocity through the projectile and target materials can be represented by [2]:

$$C_i = [(1/\rho_i)\ (d\sigma\ /\ d\epsilon)_i]^{\frac{1}{2}}\ ,\ i = P, t\ , \tag{3}$$

where ρ is the material density.

ANALYTICAL MODEL

During the perforation process, the projectile modes are: (i) plastic deformation (heading), and (ii) rigid. Whereas the target perforation stages of each projectile mode include: (a) erosion, (b) indentation, (c) plug formation, and (d) plug ejection. The perforation process is assumed to be localized. For each perforation stage, the one-dimensional impulse-momentum equation has been used to derive the equations of motion for the moving masses. A system of first order dependent differential equations representing the main equations of each perforation stage is derived. The complete perforation process consists of a combination of different stages of the different projectile modes.

Projectile Rigid Mode

The projectile is initially modelled as a flat-ended cylinder of diameter D_o and mass M_1. When the impact speed of projectile is greater than the plastic wave velocity through the target C_t, the plastic wave cannot leave the impact interface and a shock wave is generated [2]. The pressure behind the shock wave is very high. Erosion is associated with the shock wave. The projectile penetrates the target with the penetration velocity V_1. The main equations representing erosion stage are derived assuming that the plug non-deformed mass M_4 is moving with velocity V_4 [12]. If the mass M_4 is at rest, then the velocity V_4 as well as the bulge height Z_4 are set to equal zeros in the derived equations.

For impact velocity V_i less than the plastic wave velocity through the target material C_t, the indentation stage may represent the initial stage of the perforation process. Moreover, indentation stage may follow the erosion stage when the plug non-deformed mass M_4 is motionless at the end of target erosion stage. The plastic wave starts to propagate from the interface through the target material. The plastic wave divides the plug material into deformed and non-deformed masses. The deformed mass, between the plastic wave front and projectile front, moves with velocity V_3 which is equal to the projectile velocity V_1. The non-deformed mass ahead of the plastic wave front is acted on by the constrained dynamic yield stress σ_C. The ultimate shear stress τ around the plug resists the projectile motion. Once the plastic wave moves into the target, the plug deformed mass increases while its non-deformed mass decreases [12].

When the velocity of the plug non-deformed mass V_4 is greater than zero, the indentation stage terminates. Then the plug formation stage follows indentation; this stage terminates when the plastic wave propagation through the target is diminished. This occurs when the plug and the projectile move as a rigid body with the same velocity. The plug thickness is determined at the end of plug formation stage. In the plug ejection stage, the only resisting force for plug and projectile motion is the shear force. This stage terminates when the projectile reaches the back face of the target. The main equations representing the stages of target perforation by a rigid projectile are derived using the one-dimensional impulse-momentum equation [12].

The perforation stages that represent the plate perforation process by a rigid projectile are determined according to plate thickness and hardness as well as the relation between the projectile velocity and the plastic wave velocity through the target material. For example, the perforation process could consist of plug formation and plug ejection when a rigid projectile impacts into a thin plate with velocity less than the plastic wave velocity C_t. Moreover, the perforation process could consist of all the stages if a rigid projectile impacts a thick plate (i.e. $H_o/D_o > 0.5$) with velocity greater than the plastic wave velocity C_t [12].

Projectile Deformation (Heading) Mode

The rigid projectile mode is not the dominant mode during perforation. Projectile deformation is frequently observed when the target has a high hardness or when high impact velocity is involved. In the following, the perforation process of a projectile through metallic plates of thin and intermediate thicknesses has been analyzed considering the projectile deformation (heading). Due to the impact, the plastic waves propagate from the interface through the projectile and target materials, respectively. The plastic wave divides the projectile material into: (i) non-deformed mass M_1 which moves with velocity V_1, and (ii) deformed mass M_2 which moves with the interface velocity V_2. The plastic wave also divides the plug material ahead of projectile into: (a) non-deformed mass M_4 which moves with velocity V_4, and (b) deformed mass M_3 which moves with velocity equal to the velocity of the projectile deformed mass M_2. Figure 1 represents diagrammatically the perforation stages associated with the projectile deformation.

The shock wave is assumed to stand at the impact interface if the initial interface velocity V_{2o} is greater than the plastic wave velocity through the target material C_t. Erosion of the target surface accompanies the standing shock wave. Alternatively, the plastic wave propagates through the target material. The plastic wave propagation through the projectile material can be diminished during the perforation. This means that both the deformed and the non-deformed masses of the projectile move with the same velocity. Then the projectile is considered as a rigid mass during the remaining stages of the perforation process. The perforation process is then completed using the perforation stages of the projectile rigid mode [12].

Equations of motion of projectile masses

The projectile is initially modelled as a flat-ended cylinder of diameter D_o and length L_o (cf. Fig. 1). In the following, the initial relative velocity (V_1-V_{2o}) between the non-deformed mass M_1 and deformed mass M_2 of projectile is considered to be less than the plastic wave velocity through the projectile material C_P. Due to the high-speed impact, the projectile presented area on the target surface is increased due to the deformation of projectile front at the moment of impact. This initial projectile interface area A_C $(= \pi D_C^2/4)$ is assumed to be constant during the perforation stages. This area has been determined experimentally.

After time t, the equations of motion of projectile masses are:

$$\rho_P A_o (L_o - C_P t) \frac{dV_1}{dt} = - \sigma_P A_o, \qquad (4)$$

and

$$\rho_P A_o C_P t \frac{dV_2}{dt} = \sigma_P A_o + \rho_P A_o C_P (V_1 - V_2) - P, \quad (5)$$

where P is the interface force. The rate of change of length of the projectile non-deformed mass L with respect to time can be represented by:

$$\frac{dL}{dt} = - C_P . \quad (6)$$

The principle of mass conservation is applied on the total projectile mass at each incremental time Δt. Under the assumption that the projectile deformed mass has a frustum shape, the current height of the projectile deformed mass H can be predicted.

Governing equations of the target perforation stages

In the following, the one-dimensional impulse-momentum equation has been used to derive the main equations representing each perforation stage. The penetration velocity of projectile through the target is represented by the velocity of projectile deformed mass V_2. In addition, the projectile presented area on target (interface area) is denoted by A_C.

(i) Target erosion (Fig. 1a)

The projectile impact velocity at which the target surface starts to erode is denoted by V_{et}. Since the impact velocity is greater than the velocity V_{et}, a shock wave stands at the interface. The derived equations from the target analysis are:

(i) the interface force P:

$$P = \pi D_C \tau (H_o - Z) + \rho_t A_C (H_o + Z_4 - Z) \frac{dV_4}{dt} + \rho_t A_C V_2 (V_2 - V_4), \quad (7)$$

(ii) the internal force F_2:

$$F_2 = \sigma_C A_C = P - \rho_t A_C V_2 (V_2 - V_4), \quad (8)$$

(iii) the equation of motion of the plug non-deformed mass:

$$\sigma_C A_C - \pi D_C \tau (H_o - Z) = \rho_t A_C (H_o + Z_4 - Z) \frac{dV_4}{dt}, \quad (9)$$

(iv) the equation of motion of projectile deformed mass:

$$\rho_P A_o C_P t \frac{dV_2}{dt} = \sigma_P A_o + \rho_P A_o C_P (V_1 - V_2) - \sigma_C A_C - \rho_t A_C V_2 (V_2 - V_4), \quad (10)$$

(v) the rate of change of projectile penetration depth Z with respect to time:

$$\frac{dZ}{dt} = V_2 . \quad (11)$$

and (vi) the rate of change of the bulge height Z_4 with respect to time:

$$\frac{dZ_4}{dt} = V_4 . \qquad (12)$$

The force exerted by the target against the motion of projectile deformed mass (resisting force) is represented by:

$$F_R = \sigma_C A_C + \rho_t A_C V_2 (V_2 - V_4) . \qquad (13)$$

Equations (4), (6), (9), (10), (11), and (12) are a system of first order dependent differential equations that represent the current stage; this system is solved numerically. The initial conditions are:

$$at \quad t=0, \; V_1 = V_i, \; V_2 = V_{2o}, \; V_4 = 0, \; Z = 0, \; Z_4 = 0, \; L = L_o .$$

To determine the initial interface velocity V_{2o}, the above initial conditions are substituted into Eqn. (10). A second order equation is obtained; the initial interface velocity is the solution of this equation. The velocity V_{ct} is also equivalent to the projectile impact velocity when the initial interface velocity V_{2o} is equal to the wave velocity C_t.

There are three conditions to terminate this stage. The first two conditions are accompanied with the projectile deformation (i.e. $(V_1-V_2) < C_p$). These conditions are: (i) $V_3 < C_t$ and $V_4 = 0$, or (ii) $(V_3-V_4) < C_t$ and $V_4 > 0$. For condition (i), indentation follows the current stage. For condition (ii) the plug formation follows the current stage. The third condition is applied when the plastic wave propagation through the projectile material is diminished (i.e. $V_1 = V_2$). The target erosion stage of the projectile rigid mode follows the current stage [12]; the perforation process is completed by the required stages of the projectile rigid mode. The end conditions of the current stage are the initial conditions for the subsequent stage.

(ii) Indentation

Indentation can represent the initial stage of the perforation process. During indentation, the projectile mass M_2 and the plug mass M_3 move with the same velocity V_2 and the plug mass M_4 is stationary (cf. Fig .1b). The force at the plastic wave front F_2 ($=\sigma_C A_C$) and the shear force due to the ultimate shear stress acting over the surface of the plug mass M_3 resist its motion.

The main equations representing the current stage are derived assuming that it follows the target erosion stage. The derived equations are:

(i) the interface force P:

$$P = \sigma_C A_C + \pi D_C \tau (Z_1 + C_t (t-t_1) - Z) + \rho_t A_C C_t (t-t_1) \frac{dV_2}{dt} + \rho_t A_C C_t V_2 , \qquad (14)$$

and (ii) the equation of motion of projectile and plug deformed masses:

$$(\rho_P A_o C_P t + \rho_t A_C C_t (t-t_1)) \frac{dV_2}{dt} = A_o (\sigma_p + \rho_P C_P (V_1 - V_2)) - A_C (\sigma_C + \rho_t C_t V_2)$$

$$- \pi D_C \tau (Z_1 + C_t (t-t_1) - Z) , \qquad (15)$$

where t_1 is the time at which the target erosion is terminated and Z_1 is the corresponding depth of penetration. The rate of change of the projectile penetration depth Z with respect to time is represented by Eqn. (11). The force exerted by the target (resisting force) against the motion of projectile and plug deformed masses is represented by:

$$F_R = \sigma_C A_C + \pi D_C \tau (Z_1 + C_t (t - t_1) - Z) + \rho_t A_C C_t V_2 . \qquad (16)$$

Equations (4), (6), (11), and (15) are a system of first order dependent differential equations; this system is solved numerically. The end conditions of the target erosion stage are the initial conditions for the current stage. If the indentation is the initial stage for the perforation process, then the initial conditions to solve this system are:

$$at \quad t = 0, \quad V_1 = V_i, \quad V_2 = V_3 = V_{2o}, \quad Z_1 = t_1 = 0, \quad Z = 0, \quad L = L_o .$$

The initial interface velocity V_{2o} is determined using the following equation:

$$V_{2o} = \frac{\sigma_P A_o + \rho_P A_o C_P V_i - \sigma_C A_C}{\rho_P A_o C_P + \rho_t A_C C_t} . \qquad (17)$$

Two conditions terminate this stage: (i) $(V_1 - V_2) < C_P$ and $V_4 > 0$, or (ii) $(V_1 - V_2) = 0$ and $V_4 = 0$. For condition (i), the plug formation stage of the projectile heading mode follows indentation. For condition (ii), the indentation of the projectile rigid mode follows the current stage; the remaining stages of the perforation process are then completed using the corresponding perforation stages of the projectile rigid mode [12].

(iii) Plug formation

In the following, the plug formation is described assuming that it follows the target erosion then indentation. The plug non-deformed mass M_4 starts to move with velocity V_4; the bulge protrudes from the back face of the plate (cf. Fig. 1c). The derived equations that represent the current stage are:

(i) the interface force P:

$$P = \pi D_C \tau (H_o - Z) + \rho_t A_C [(H_o + Z_4 - Z_1 - C_t (t - t_1)) \frac{dV_4}{dt} + C_t (V_2 - V_4) + C_t (t - t_1) \frac{dV_2}{dt}] \qquad (18)$$

(ii) the internal force F_2:

$$F_2 = \sigma_C A_C = P - \pi D_C \tau (Z_1 + C_t (t - t_1) - Z) - \rho_t A_C C_t (t - t_1) \frac{dV_2}{dt} - \rho_t A_C C_t (V_2 - V_4) , \qquad (19)$$

(iii) the equation of motion of plug non-deformed mass M_4:

$$\rho_t A_C (H_o + Z_4 - Z_1 - C_t (t - t_1)) \frac{dV_4}{dt} = -\pi D_C \tau (H_o - C_t (t - t_1) - Z_1) + \sigma_C A_C , \qquad (20)$$

and (iv) the equation of motion of projectile and plug deformed masses:

$$[\rho_P A_o C_P t + \rho_t A_C C_t (t - t_1)] \frac{dV_2}{dt} = A_o [\sigma_P + \rho_P C_P (V_1 - V_2)] - \rho_t A_C C_t (V_2 - V_4)$$

$$- \sigma_C A_C - \pi D_C \tau [Z_1 + C_t (t - t_1) - Z] . \qquad (21)$$

Equations (11), and (12) represent the rate of change of the projectile penetration depth Z and bulge height, respectively, with respect to time. The force exerted by the target against the motions of the projectile and the plug deformed masses is represented by:

$$F_R = \sigma_C A_C + \rho_t A_C C_t (V_2 - V_4) + \pi D_C \tau (Z_1 + C_t (t - t_1) - Z) . \qquad (22)$$

Equations (4), (6), (11), (12), (20), and (21) are a system of first order dependent differential equations that represent the current stage; this system is solved numerically. The end conditions of target erosion stage or indentation are the initial conditions for the present stage. If the plug formation is the initial stage of the perforation process, then the initial conditions are:

$$at \quad t = 0, \quad V_1 = V_i, \quad V_2 = V_3 = V_{2o}, \quad V_4 = 0, \quad Z_1 = t_1 = 0, \quad Z = Z_4 = 0, \quad L = L_o,$$

and the initial interface velocity V_{2o} is determined using Eqn. (17).

There are two conditions to terminate this stage: (i) $(V_1 - V_2) < C_P$ and $V_3 = V_4$, or (ii) $V_1 = V_2$ and $(V_3 - V_4) > 0$. For condition (i), the plug ejection stage considering the projectile deformation follows the current stage and the plug thickness H_b ($= H_o + Z_4 - Z$) is determined at the end of plug formation stage. For condition (ii), the plug formation stage of the projectile rigid mode follows the current stage [12]; the plug thickness is determined when the plug formation stage is completely terminated. Then the plug ejection stage of projectile rigid mode completes the perforation process. The end conditions of this stage are the initial conditions for the subsequent stage.

(iv) Plug ejection

In this stage, the only resisting force for the motions of the projectile deformed mass and ejected plug is the shear force. Figure 1d shows the projectile masses, the ejected plug, their velocities and the associated forces. The main derived equations of the current stage are:
(i) the interface force P:

$$P = \pi D_C \tau (H_o - Z) + \rho_t A_C (H_o - Z_1) \frac{dV_2}{dt} , \qquad (23)$$

and (ii) the equation of motion of the projectile deformed mass and ejected plug:

$$(\rho_P A_o C_P t + \rho_t A_C (H_o - Z_1)) \frac{dV_2}{dt} = A_o (\sigma_P + \rho_P C_P (V_1 - V_2)) - \pi D_C \tau (H_o - Z) . \qquad (24)$$

The rate of change of the projectile penetration depth Z with respect to time is represented by Eqn. (11). The target resisting force is determined by the following equation:

$$F_R = \pi D_C \tau (H_o - Z) . \qquad (25)$$

Equations (4), (6), (11), and (24) are a system of first order dependent differential equations; these are solved numerically. There are two conditions to terminate this stage: (i) $Z = H_n$ and $(V_1-V_2) < C_p$, or (ii) $Z < H_n$ and $V_1 = V_2$. For condition (i), the perforation process is terminated while the projectile front is still plastically deformed. For condition (ii), the plug ejection stage of the projectile rigid mode follows the current stage [12]. The end conditions of the present stage are the initial conditions for the subsequent stage.

The model essentially contains two projectile modes. The complete perforation process can be represented individually by the stages of projectile rigid mode if the projectile is assumed to be rigid during target perforation [12], or by a combination of the different perforation stages associated with the different projectile modes. When the stages of projectile rigid mode follow the stages of heading mode, the main equations for the required stages of projectile rigid mode are used after replacing the interface area A_n by the projectile presented area on target A_C. The main equations of the different perforation stages associated with the different projectile modes are programmed using FORTRAN. The program deals with the projectile impact into metallic plates of finite thicknesses over a wide range of impact velocity. To utilize the perforation stages associated with the projectile heading modes, the change of projectile interface area with impact velocity should be fed into the program.

RESULTS AND DISCUSSIONS

In the following, the post perforation velocities predicted by the model are compared with the experimental measurements of other investigators. Predicted samples of the model results are presented and discussed. The present results are classified into: (i) validation of the model, and (ii) predictions. Moreover, the influence of the projectile deformation consideration during perforation process on the predicted model results is presented and discussed.

(i) Validation of the Model

Woodall et al. [13] gave brief data of post perforation examinations of 4130 steel projectiles that perforate 6.35 mm thick 2024-T3 aluminium plates at two different impact velocities. Because of the lack of data, the interface area is assumed to be linear with impact velocity. The program is run to predict the post perforation velocities due to the impact of steel projectiles of calibre 7.82 mm and length of 19.58 mm into aluminium plates at different impact velocities. The Brinell hardness number of projectile material is 325 HB.

Fig. 2 shows the projectile residual velocities measured by Woodall et al. [13] and the corresponding results predicted using the present model versus projectile impact velocity. The predicted residual velocities considering the projectile rigidity during perforation are also depicted on the same figure. The model predictions of projectile residual velocities are in good agreement with experimental measurements obtained by Woodall et al. when the projectile deformation is considered.

Another validation of the present model is done by comparing the experimental measurements of projectile residual velocities obtained by Yuan et al. [8] with the model predictions. They used 1045 and 1020 steel projectiles to impact LY12-CZ aluminium alloy plates of different thicknesses with different impact velocities. The 1045 steel projectile has a calibre of 4.96 mm, a length of 12.2 mm and a Brinell hardness number of 160 HB, whereas the 1020 steel projectile has a calibre of 6.13 mm,

a length of 6.15 mm and a Brinell hardness number of 110 HB. The LY12-CZ aluminium alloy plates have thicknesses of 3 and 5 mm, respectively, and Brinell hardness numbers of 62 HB.

The 3 mm thick aluminium alloy plates were perforated by 1045 steel projectiles, whereas the 5 mm thick aluminium alloy plates were perforated by 1020 steel projectiles. Yuan et al. [8] determined experimentally the change of the projectile interface area A_C with projectile impact velocity for both 1045 and 1020 steel projectiles over their used impact velocity range. For 3 mm thick aluminium alloy plates, Fig. 3a plots the projectile residual velocities measured by Yuan et al. [8] and the corresponding predicted ones using the present model, whereas Fig 3b depicts the measured projectile residual velocities by Yuan et al. [8] and the corresponding model predictions for 5 mm thick aluminium alloy plates. The computed results considering the projectile rigidity during perforation are also depicted on their respective figures. A good agreement is obtained between the Yuan et al. [8] experimental measurements and the model predictions when the projectile deformation is considered.

From the previous validations of the model results, it seems that the model is capable of predicting good post-perforation results when the projectile deformation is considered. Actually, the projectile front is subjected to plastic deformation during the perforation process. This deformation appears when the projectile impacts into a metallic plate of high hardness with high velocity. The projectile deformation has a significant influence on the perforation process and cannot be neglected in the analysis.

(ii) Predictions and Discussions

In the following, the results of the present model due to the impact of steel projectiles into aluminium alloy plates of two thicknesses with different impact velocities are presented. The analytical results are predicted using the data for projectile and target that were tested by Yuan et al. [8]. The input data to the computer program are listed in Table 1.

Because of the high impact velocity and/or plate hardness and thickness, the projectile front is subjected to plastic deformation. The interface area of the projectile front increases with projectile impact velocity. In order to apply the projectile heading mode of the present model, it is necessary to determine experimentally the projectile interface area for each projectile impact velocity into each plate thickness. The measured interface area A_C by Yuan et al. divided by the original cross-sectional area of the projectile A_o has been related to the projectile impact velocity using a quadratic empirical equation. This equation is fed into the program; it is represented as follows:

$$(A_C / A_o) = A + B V_i + C V_i^2, \qquad (26)$$

where A, B and C are constants. Table 2 lists the values of the equation constants due to the impact of steel projectiles into 3 and 5 mm thick aluminium alloy plates, respectively.

Figures 4a and 4b depict the force-time histories for 3 and 5 mm thick LY12-CZ aluminium alloy plates at different impact velocities. It is obvious from these figures that the maximum target resisting force against projectile penetration increases with impact velocity. For each plate thickness, the projectile interface velocity V_2 and the interface area A_C increase with the increase in projectile impact velocity. The target deformation rate increases, and consequently its resistance, with the increase in projectile interface velocity and interface area.

Table 1. Input data to the computer program

Ser. No.	Parameter	Plate thickness, H_o [mm]	
		3	5
1	Projectile material code	SAE 1045	SAE 1020
2	Projectile diameter, D_o [mm]	4.96	6.13
3	Projectile length, L_o [mm]	12.2	6.15
4	Projectile density, ρ_P [kg/m^3]	7850	7850
5	Projectile hardness, [HB]	160	110
6	Impact velocity range, [m/s]	up to 650	up to 650
7	Projectile interface area ratio	According to Eqn. (26)	
8	Target material code	LY12-CZ Al. alloy plates	
9	Target density, ρ_t [kg/m^3]	2750	
10	Target hardness, [HB]	62	

Table 2. Values of equation constants that determinate the projectile interface area ratio as a function of impact velocity.

Plate thick. H_o [mm]	Constant values		
	A [s^2/m^2]	B [s/m]	C
3	1.062	7.142E-6	9.286E-7
5	0.709	1.58E-3	-7.057E-7

The target resisting force is maximum when the projectile starts to penetrate the plate and then the force slightly decreases. The plug non-deformed mass moves with velocity V_4. At the moment in which the velocity of the plug non-deformed mass equals the interface velocity V_2, the force suddenly drops due to the diminishing of the plastic wave through the plug material. The only resisting force at this moment is the shear force along the plug periphery and this force vanishes when the projectile front reaches the back face of the target.

The velocity ratios-time histories of the projectile masses and plug masses during the perforation process of the 3 mm thick LY12-CZ aluminium alloy plates at impact velocities of 400 and 500 m/s are shown in Fig. 5a. The perforation process of the 3 mm thick aluminium alloy plates successively consists of plug formation followed by plug ejection of the projectile heading mode and plug ejection of the projectile rigid mode. The plug formation of the projectile heading mode

represents the initial stage of the perforation process. This stage terminates when the velocity of the plug non-deformed mass V_4 is equal to the projectile interface velocity $V_2(= V_3)$. The plug formation stage takes a long time when the impact velocity is 500 m/s; this is because the penetration velocity is high and the plug non-deformed mass needs a long time until it moves with the current penetration velocity. Moreover, the projectile rigid mass M_1 moves with velocity V_1 which is greater than the projectile interface velocity V_2.

The plug ejection stage of the projectile heading mode follows the initial perforation stage. This stage continues until the plastic wave through the projectile material diminishes (i.e. $V_1 = V_2 = V_4$). Then the projectile and ejected plug move as a rigid mass; the plug ejection stage of the rigid projectile completes the perforation process. The only resisting force during the plug ejection stages of the projectile heading and rigid modes is the shear force along the plug periphery. The perforation process is terminated when the projectile front reaches the back face of the target.

The velocity ratios-time histories of the projectile masses and the plug masses during the perforation process of the 5 mm thick LY12-CZ aluminium alloy plate at an impact velocity of 500 m/s are shown in Fig. 5b. At this particular impact velocity, the perforation process also consists of plug formation followed by plug ejection of the projectile heading mode and plug ejection of the projectile rigid mode. Comparing the present figure with the previous one, Fig. 5a, the trend of the velocities of projectile masses as well as plug masses generally does not change with the change of plate thickness.

The time histories of the projectile penetration depth are also predicted. The projectile penetration depth-time histories due to the impact of the 3 mm thick LY12-CZ aluminium alloy plates with different velocities are shown in Fig. 6a. It is clear that the projectile penetration depth increases with the increase of impact velocity. In addition, the perforation time decreases by increasing the impact velocity. This is attributed to the increase of penetration velocity of projectile with impact velocity. In addition, Fig. 6b depicts the predicted time histories of projectile penetration depth due to the impact of the 5 mm thick LY12-CZ aluminium alloy plates with different velocities. The trend of projectile penetration depth does not change with plate thickness.

Effect of Projectile Deformation on Predicted Time-Histories and Post-Perforation Results

Figure 7a shows the predicted time-history of target resisting force for a 3 mm thick LY12-CZ aluminium alloy plate when the projectile deformation is considered during penetration. The projectile impacts into the plate with a velocity of 400 m/s. Similarly, Fig. 7b shows the force-time history for a 5 mm thick LY12-CZ aluminium alloy plate at an impact velocity of 600 m/s. The predicted time-histories of target resisting force for 3 and 5 mm thick aluminium alloy plates when the projectile is assumed to be rigid during penetration are depicted on their respective figures.

For the deformed projectile, it is clear from both figures that the target resisting force has the highest value when the projectile penetration starts. This is attributed to the increase of projectile interface area due to the deformation of projectile front. In addition, the impulse exerted by the target ($= \int F(t)\, dt$) against projectile penetration is high. Thus the decrease in projectile velocity is more when the projectile deformation is considered during penetration.

The deformed projectile takes more time than the rigid projectile to reach the backface of the plate. This is due to the low penetration velocity in comparison with the penetration velocity when the rigid projectile penetrates the target. When the projectile deformation is considered during penetration, the penetration velocity is represented by the velocity of the deformed part of projectile which is in-contact with target.

For the deformed projectile, Fig. 8a shows the velocity ratio-time history of the projectile rigid mass due to the impact of the 3 mm thick aluminium alloy plate with a velocity of 600 m/s. In addition, the corresponding predicted velocity ratio-time history of the rigid projectile is plotted on the same figure. For the deformed projectile, the force that resists the motion of its rigid mass is represented by the multiplication of the stress at the plastic wave front through the projectile material into its original cross-sectional area. Moreover, the force that resists the rigid projectile penetration is represented by the target resisting force.

The rigid mass of the deformed projectile which moves with velocity V_1 is denoted by $\rho_p A_o(L_o - C_p t)$; whereas the mass that moves with the same velocity when the rigid projectile penetrates the target is denoted by $M_t + \rho_t A_o C_p(t-t_1)$. The rigid mass of the deformed projectile always decreases during penetration while the mass that moves with velocity V_1 for the case of rigid projectile increases. Moreover, the force resisting the rigid mass motion of the deformed projectile is always greater than the target resisting force when the rigid projectile penetrates the target; this is due to the high hardness of projectile material. Therefore, the deceleration of the rigid mass of deformed projectile is greater than the deceleration of the masses that move with velocity V_1 for the case of rigid projectile. This leads to the low velocity of the rigid mass of deformed projectile in comparison with the velocity of the rigid projectile at any particular time during perforation. In addition, the penetration velocity of rigid projectile is greater than the corresponding one when the deformed projectile penetrates the target. Thus the deformed projectile takes a long time to reach the backface of the plate.

Figure 8b shows the velocity ratio-time history of the rigid mass of deformed projectile due to the impact of a 5 mm thick LY12-CZ aluminium alloy plate with a velocity of 400 m/s. In addition, the corresponding predicted velocity ratio-time history for the rigid projectile is plotted on the same figure. It is clear that the rigid mass velocity of the deformed projectile is higher than the velocity of the rigid projectile at the earlier stages of target perforation. The force that resists the rigid mass motion of the deformed projectile is small in comparison with the target resisting force against the penetration of rigid projectile. The small resisting force in case of the deformed projectile is attributed to the low hardness of projectile.

For the deformed projectile, the time histories of projectile penetration depths due to the impact of 3 and 5 mm thick LY12-CZ aluminium alloy plates with a velocity of 500 m/s are predicted. For the 3 mm thick aluminium alloy plate, the time history of projectile penetration depth is plotted in Fig. 9a; whereas Fig 9b shows the time history of penetration-depth through a 5 mm thick aluminium alloy plate. The time history of penetration depth when the projectile is assumed to be rigid during the penetration of 3 and 5 mm thick aluminium alloy plates are predicted and plotted on their respective figures. From both figures, it is evident that the depth of penetration for the rigid projectile is always higher than that predicted for the deformed projectile. This is attributed to the high penetration velocity when the rigid projectile penetrates the target. In addition, the penetration time taken by the deformed projectile is higher than the corresponding one taken by the rigid projectile.

Figure 10 shows the predicted change of projectile velocity drop ΔV ($= V_i - V_r$) with projectile impact velocity for 3 and 5 mm thick LY12-CZ aluminium alloy plates when projectile deformation is considered during penetration. In addition, the corresponding predicted curves when the projectile is assumed to be rigid during penetration are depicted on the same figure. For both rigid and deformed projectiles, the curves show that the velocity drop ΔV decreases beyond the ballistic limit and slightly increases again with the increase of impact velocity. These results are consistent with those of other investigators such as Liss and Goldsmith [14] and Awerbuch and Bodner [15].

At low impact velocity, the target deformation may be concentrated into the shear zone during penetration process. A great amount of heat generates on the plug shearing area and the projectile may lose a low velocity to perforate the target. By increasing the impact velocity, the target resisting force increases and the energy necessary to defeat the target is high. Thus the projectile loses more velocity during perforation and the velocity drop increases. For each plate thickness, the velocity drop when the projectile deformation is considered during penetration is always higher than the corresponding one when the rigid projectile penetrates the target. This is attributed to the impulse exerted by the target against projectile penetration which is high when the deformed projectile penetrates the target.

CONCLUSIONS

An analytical model has been developed to describe the perforation process of finite thickness metallic plates by deformable projectiles. The model identifies two modes for projectile: deformation and rigid. Both projectile and target materials are assumed to be strain rate independent and to follow the rigid-linear work hardening constitutive equation with respect to their nominal stress-engineering strain relationships. The perforation process is assumed to be localized and it consists of a combination of different perforation stages of the different projectile modes. For each plate thickness, the change of projectile interface area with impact velocity should be fed into the model; this change is determined experimentally. The model is capable of predicting the time-histories of the velocities of projectile masses and plug masses, projectile penetration depth, and target resisting force. It can also predict the projectile residual velocity, plug thickness, and the final length of projectile after perforation.

Representative analytical results using the developed perforation model have been introduced. In addition, the model is used to study the effect of projectile deformation during penetration on its predicted results. During the analysis of the model results, it is shown that:

(i) for high projectile impact velocities and high plate hardness, projectile deformation should be considered in the analysis of perforation.

(ii) The present model can deal with all possibilities of projectile encountering with a finite metallic plate which result in a plate plugging failure up to impact velocity less than the transient velocity (impact velocity at which the projectile front starts to erode).

(iii) The model predictions are in good agreement with available experimental measurements when the projectile deformation is considered in the analysis.

(iv) The projectile interface area and the penetration velocity have a great influence on the predicted time histories of target resisting force, velocities of moving masses and depth of penetration as well as the total time of perforation process. The increase of the interface area leads to an increase in projectile deceleration and total time of perforation process.

REFERENCES

1. Recht, R.F. and Ipson, T.W., 'Ballistic Perforation Dynamics', J. Appl. Mech., Vol. 30, pp. 384-390 (1963).
2. Recht, R.F., 'Taylor Ballistic Impact Modelling Applied to Deformation and Mass Loss Determination', Int. J. Engng. Sci., Vol. 16, pp. 809-827 (1978).
3. Taylor, G.I., 'The Use of Flat Ended Projectiles for Determining Dynamic Yield Stress', Proc. R. Soc., London, England, A194, pp. 299-299 (1948).
4. Awerbuch, J., 'A Mechanics Approach to Projectile Penetration', Israel J. of Technology, Vol. 8, No. 4, pp. 375-383 (1970).

5. Awerbuch, J. and Bodner, S.R., 'Analysis of the Mechanics of Perforation of Projectiles in Metallic Plates', Int. J. Solids Struct., Vol. 10, pp. 671-684 (1974).
6. Liss, J., Goldsmith, W. and Kelly, J.M., 'A Phenomenological Penetration Model of Plates', Int. J. Impact Engng., Vol. 1, pp. 321-341 (1983).
7. Ravid, M. and Bodner, S.R., 'Dynamic Perforation of Visco-plastic Plates by Rigid Projectiles', Int. J. Engng. Sci., Vol. 21, pp. 577-591 (1983).
8. Yuan, W., Lanting, Z., Xiaoging, M. and Stronge, W., 'Plate Perforation by Deformable Projectiles-A Plastic Wave Theory', Int. J. Impact Engng., Vol. 1, pp. 393-412 (1983).
9. Lee, E.H. and Wolf, H., 'Plastic-Wave Propagation in High-Speed Testing', J. Appl. Mech., Vol. 18, pp. 379-386 (1951).
10. Woodward, R.L. and De Morton, M.E., 'Penetration of Targets by Flat-Ended Projectiles', Int. J. Mech. Sci., Vol. 18, pp. 119-127 (1976).
11. Liss, J., Goldsmith, W. and Hauser, F.E., 'Constraint to Side Flow in Plates', J. Appl. Mech., Vol. 50, pp. 694-698 (1983).
12. Riad, A.M. and Leech, C.M., 'An Investigation of Metallic Plate Perforation by Rigid Projectiles using Plastic Wave Theory', 2 nd International Conf. on Applied Mech. and Mech. Engng., Vol. 1, pp. 137-159 (1994).
13. Woodall, S.R., Heyda, J.F., Galbraith, H.J. and Wilson, L.L., 'Ballistic Impact Mechanics of Selected Metallic and Composite Materials', Technical report AFATL-TR-70-112, Book I and II, Eglin Air Force Base (Nov. 1970).
14. Liss, J. and Goldsmith, W., 'Plate Perforation Phenomena Due to Impact by Blunt Cylinder', Int. J. Impact Engng., Vol. 2, pp. 37-64 (1984).
15. Awerbuch, J. and Bodner, S.R., 'Expermental Investigation of Normal Perforation of Projectiles in Metallic Plates', Int. J. Solids and Struct., Vol. 10, pp. 685-699 (1974).

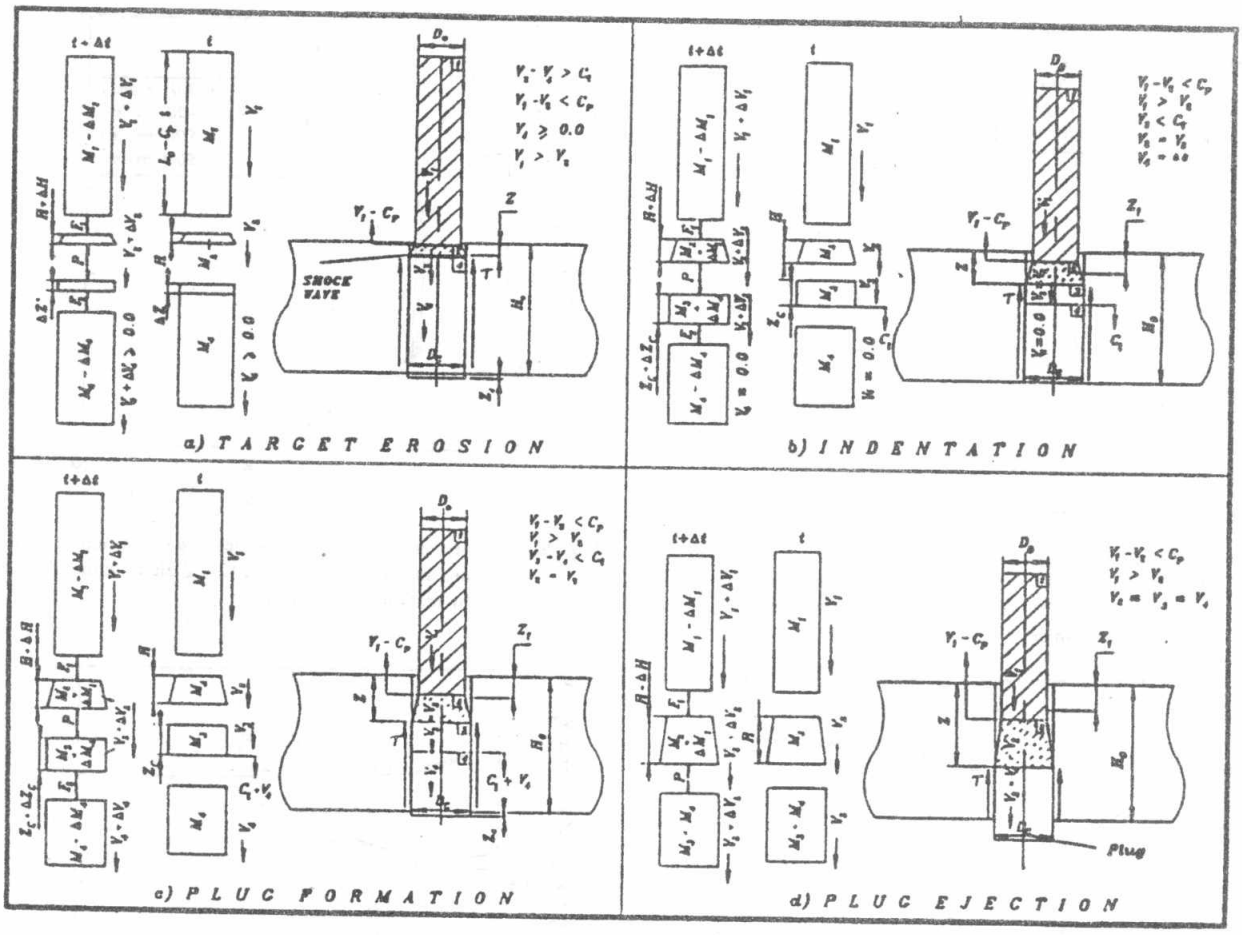

Fig. 1. Schematic diagram for the perforation stages associated with the projectile deformation showing the projectile masses, the plug masses, the velocities, and the associated forces.

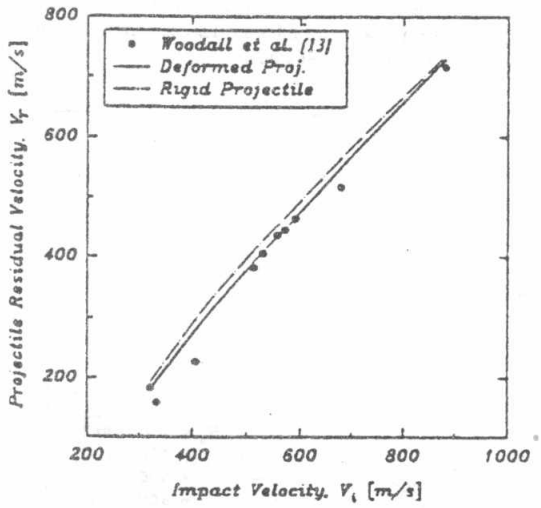

Fig. 2. The predicted change of the projectile residual velocity with impact velocity. Experimental results were obtained by Woodall et al. [13].

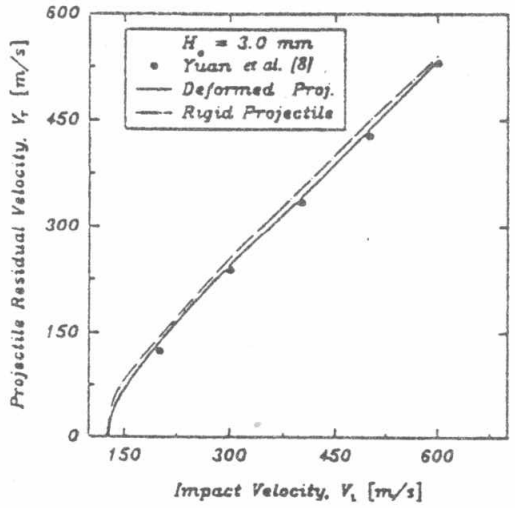

Fig. 3a. The predicted change of the projectile residual velocity with impact velocity due to the impact of 3 mm thick aluminium alloy plates by 1045 steel projectiles. Experimental results were obtained by Yuan et al. [8].

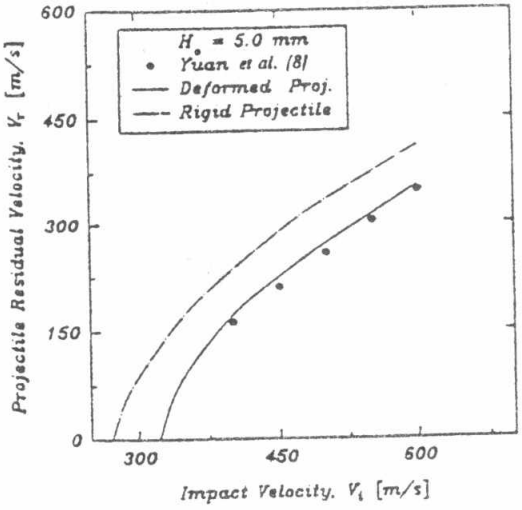

Fig. 3b. The predicted change of the projectile residual velocity with impact velocity due to the impact of 5 mm thick aluminium alloy plates by 1020 steel projectiles. Experimental results were obtained by Yuan et al. [8].

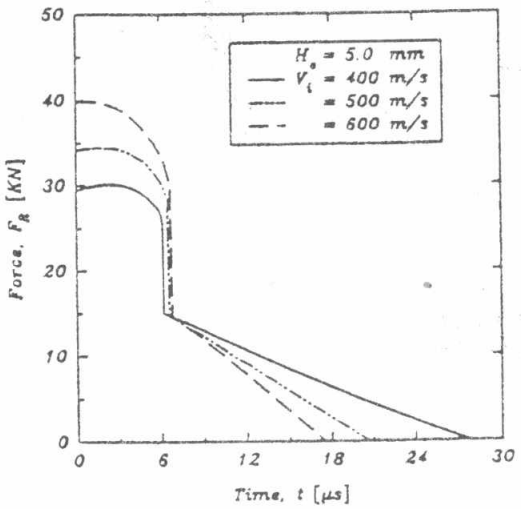

Fig. 4b. The predicted force-time histories due to the impact of a steel projectile into a 5 mm thick LY12-CZ aluminium alloy plate with different impact velocities.

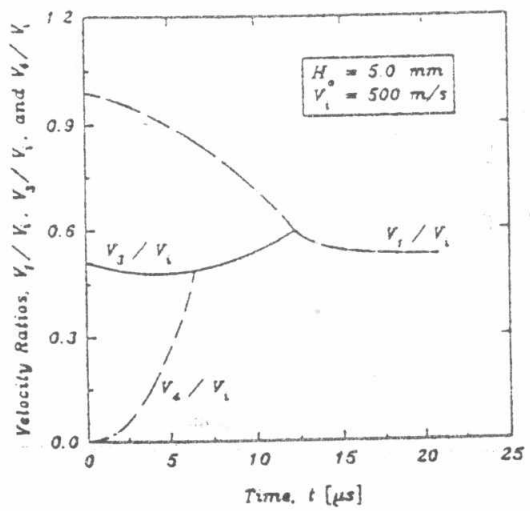

Fig. 5b. The predicted velocity ratios-time histories due to the impact of a projectile into a 5 mm thick LY12-CZ aluminium alloy plate with a velocity of 500 m/s.

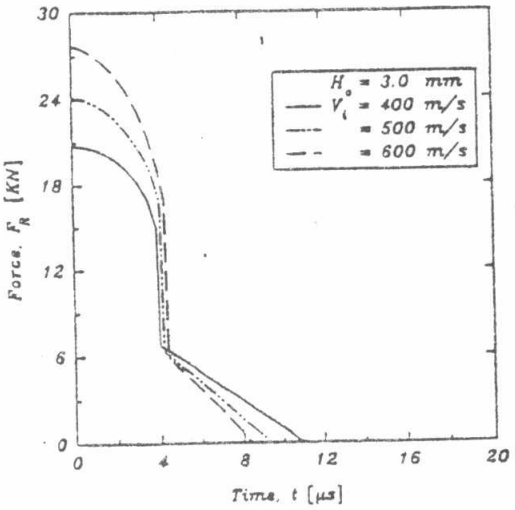

Fig. 4a. The predicted force-time histories due to the impact of a steel projectile into a 3 mm thick LY12-CZ aluminium alloy plate with different impact velocities.

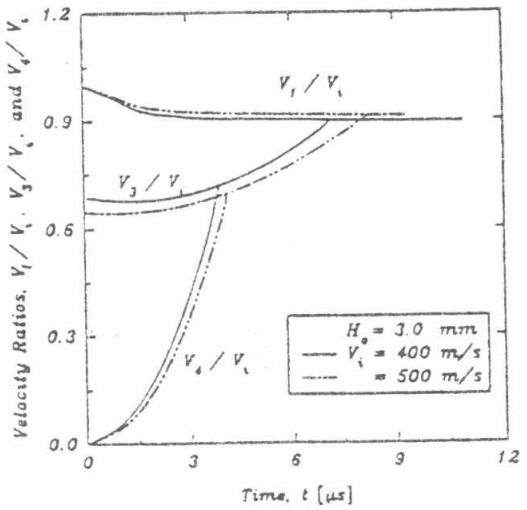

Fig. 5a. The predicted velocity ratios-time histories due to the impact of a projectile into a 3 mm thick LY12-CZ aluminium alloy plate with different impact velocities.

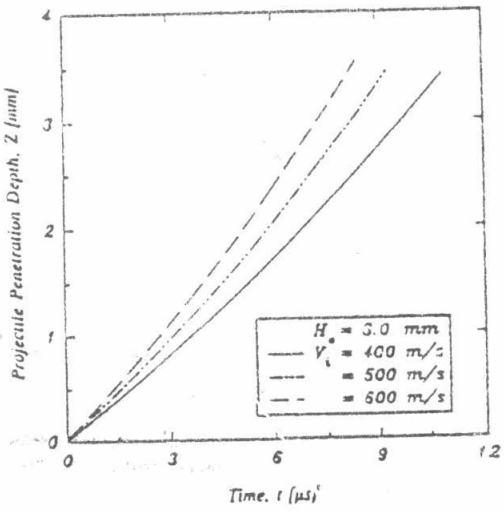

Fig. 6a. The predicted projectile penetration depth-time histories due to the impact of a steel projectile into a 3 mm thick LY12-CZ aluminium alloy plate with different impact velocities.

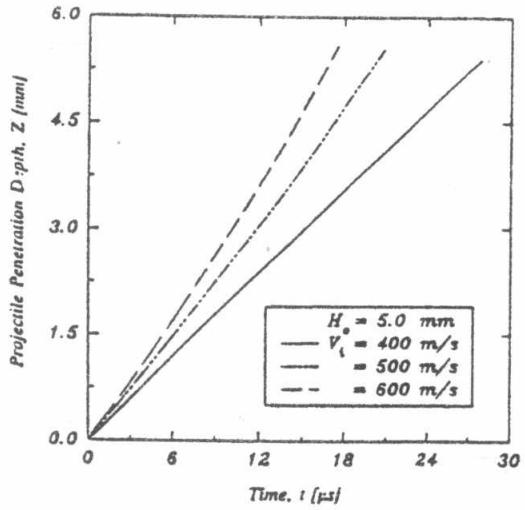

Fig. 6b. The predicted projectile penetration depth-time histories due to the impact of a steel projectile into a 5 mm thick LY12-CZ aluminium alloy plate with different impact velocities.

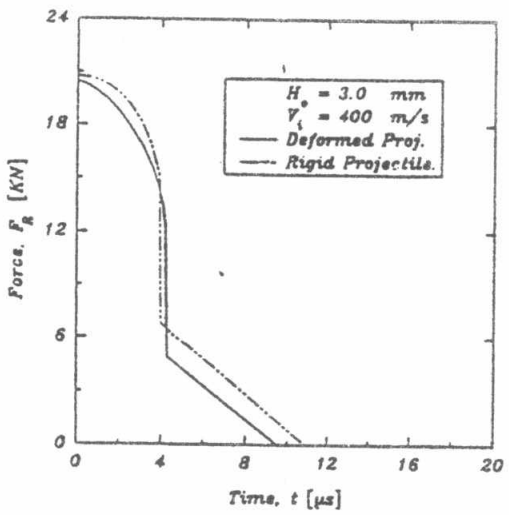

Fig. 7a. The predicted force-time histories due to the impact of a rigid and deformed steel projectiles into 3 mm thick LY12-CZ aluminium alloy plates with an impact velocity of 400 m/s.

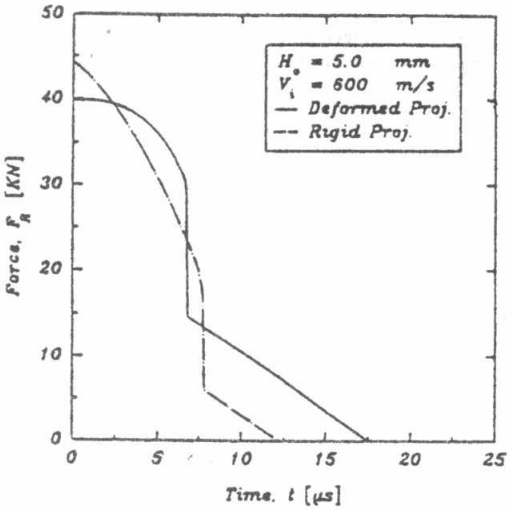

Fig. 7b. The predicted force-time histories due to the impact of a rigid and deformed steel projectiles into 5 mm thick LY12-CZ aluminium alloy plates with an impact velocity of 600 m/s.

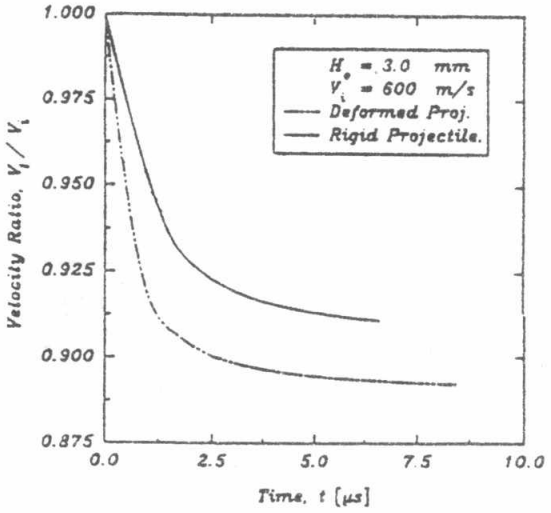

Fig. 8a. The predicted velocity ratio (V_r/V_i)-time histories for rigid projectile and rigid mass of deformed projectile due to the impact of a 3 mm thick LY12-CZ aluminium alloy plate with a velocity of 600 m/s.

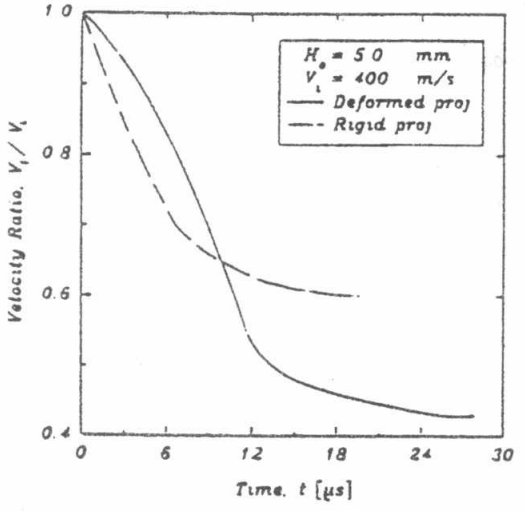

Fig. 8b. The predicted velocity ratio (V_r/V_i)-time histories for rigid projectile and rigid mass of deformed projectile due to the impact of a 5 mm thick LY12-CZ aluminium alloy plate with a velocity of 400 m/s.

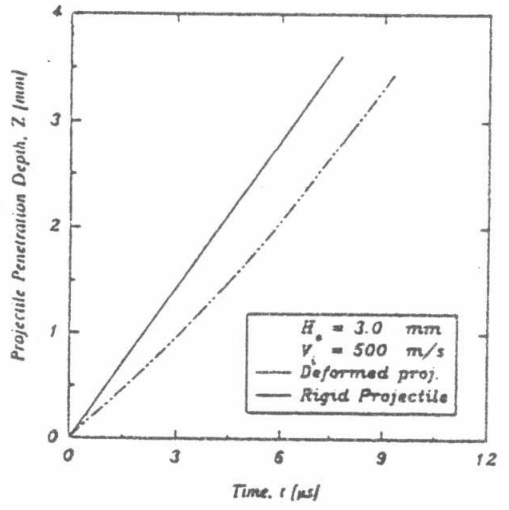

Fig. 9a. The predicted penetration depth-time histories for the rigid projectile and rigid mass of deformed projectile due to the impact of a 3 mm thick LY12-CZ aluminium alloy plate with a velocity of 500 m/s.

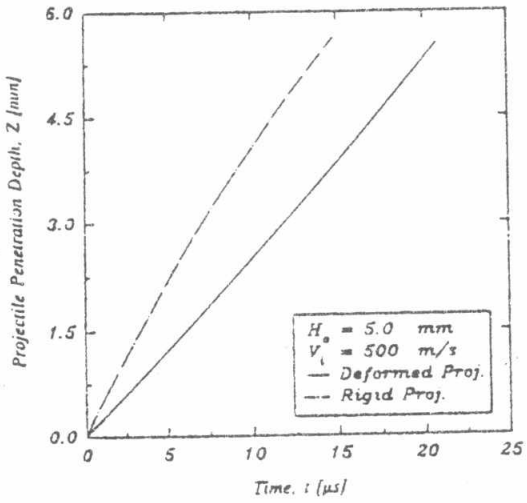

Fig. 9b. The predicted penetration depth-time histories for the rigid projectile and rigid mass of deformed projectile due to the impact of a 5 mm thick LY12-CZ aluminum alloy plate with a velocity of 500 m/s.

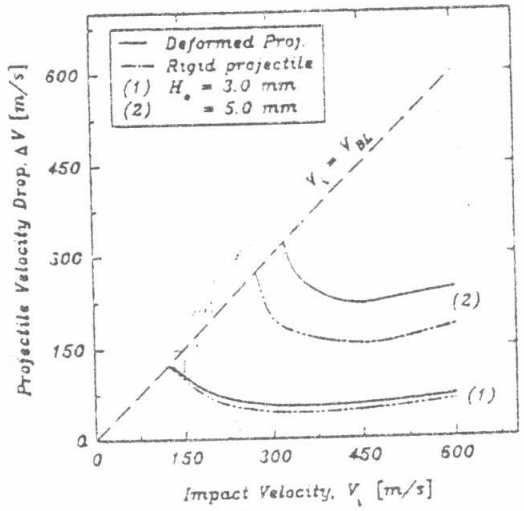

Fig. 10. The predicted change of velocity drop with projectile impact velocity for 3 and 5 mm thick LY12-CZ aluminium alloy plates. The velocity drop is predicted considering projectile deformation and projectile rigidity during the perforation process.